Applied Mathematics & Information Sciences
*An International Journal*

http://dx.doi.org/10.12785/amis/090437

# Automatic Threshold Level Set Model Applied on MRI Image Segmentation of Brain Tissue

*Ming Zhao*[1,*], *Hsiao-Yu Lin* [2], *Chih-Hung Yang*[2], *Chih-Yu Hsu*[3], *Jeng-Shyang Pan*[1] *and Meng-Ju Lin*[4]

[1] Department of computer science and technology, Harbin Institute of Technology Shenzhen Graduate School, Shenzhen , P.R.China
[2] Department of Applied Mathematics, National Chung Hsing University, Taichung, Taiwan
[3] Department of Information & Communication Engineering, ChaoYang University of Technology, Taichung, Taiwan
[4] Department of Applied Mathematics, TungHai University, Taichung, Taiwan

Received: 7 Nov. 2014, Revised: 7 Feb. 2015, Accepted: 8 Feb. 2015
Published online: 1 Jul. 2015

**Abstract:** In the paper, a mathematical proof is given for a different mean of Chan and Vese model. Based on the proof, an image segmentation method called Automatic Threshold Level Set Without Edge was developed for the extraction of tissues in brain MR images. Thresholds are defined to find the boundary of tissues in the brain and they can be automatically obtained by Fuzzy C Mean algorithm. A similarity index (SI) is used for quantitative evaluation of the segmentation results. By testing MRI brain slice images and comparing to the ground truth of tissue segmentation, the mean and the variance of SI are 0.90311 and 0.042049. The experimental results demonstrate our method can automatically and accurately segment the regions of tissues in brain.

**Keywords:** Level Set Method, Fuzzy Clustering, Image Segmentation, Mr Imaging

## 1 Introduction

Magnetic resonance Imaging (MRI) is useful medical diagnostic tool for disease treatment or surgical planning. Segmentation of magnetic resonance images is widely applied in brain tissue classification for functional researches, radiological evaluation and 3D visualizations. Brain image segmentations classify the voxels into three different tissue types: grey matter (GM), white matter (WM), and cerebrospinal fluid (CSF). Three categories of segmentation methods [1] are edge based, region based and pixel based methods. Edge based methods use the gradient information of the intensity of images. Region based methods use intensity information in regions. Pixel based method such as the neural network classifiers used intensity as the features for classification [2,3,4,5]. The k-nearest neighbour classifier [6] and standard fuzzy c-means algorithm [7,8] are also pixel based methods. Besides active contour model [9] is edge-based method to extract the regions of interest (ROI) from primitive image by the contours of the ROI pixels. Geometric Active Contour model known as level set method [10,11] has recently been applied on the application of segmentation [12]. Level set methods are segmentation techniques to find the object contours with the advantage for automatically splitting or merging the contours [13]. The boundaries of objects are contours of level set function with zero level and the solution can be obtained by either solving a partial differential equation or optimizing an objective functional. A region based image segmentation model [14] with a piecewise smooth function fitted to the image data and the discontinuities happening only on the boundaries between different tissue types is proposed to find the object boundaries. Threshold Level Set Method [15,16] is a region based level set model by threshold selection as the boundaries of intensity intervals to separate the image regions. Our previous work [17] used Otsu [18] algorithm to automatically obtain two thresholds of speed functions for the Threshold Level Set. However, Threshold Level Set with Otsu algorithm finding crisp thresholds, the method is not available for the fuzziness of boundary. To improve the Threshold Level Set Method, a new segmentation method based on the new mean of Chan and Vese model [19] and Fuzzy C-Means algorithm is proposed. The proposed method is called Automatic Threshold Level Set Without Edge (ATLSWE) Model. By using similarity index and comparing to the ground truth of image segmentations,

* Corresponding author e-mail: hitmzhao@gmail.com

the segmentation results of the brain tissues by proposed method are accurate enough. We hope the other researchers use their programs and parameters to compare their results with the ground truth segmentations and our results.

## 2 Image Segmentation of Brain Tissues

Accuracy evaluation is the most important issue for any new segmentation method. It is very popular for researchers to evaluate their developed method by comparing with other methods. They use their own image sources segmented by their method to compare with the other methods to evaluate the accuracy of their proposed segmentation method. However, they implement the programs for the other methods and select parameters by themselves. It is not fair if they do not succeed the best segmentations when they implemented other methods with no optimal parameters. The comparisons and evaluations are unfair under these situations. It is necessary to find a common accuracy evaluation method that is fair for any new developed algorithm. Since the mrGray software package and the open source code is distributed on the Internet [20,21] and it provides brain MRI images and the results of WM segmentation. Using these segmentation results as a common ground truth is reasonable for evaluating any segmentation method for brain WM in the MRI images. MrGray software package has a T1-weighted volumetric MR image data set with DICOM format. The data set has 134 slices of MR brain images with the resolution size 204×120 pixels and the gray level ranging from 0 to 255. The resolution of the data set is fine enough to resolve the complex structure of the cortex and to provide adequate contrast between GM, WM, and CSF. The segmentation results of the WM are also provided in mrGray software package which are used as ground truth to be compared with the segmentation results by the ATLSWE model. The image pre-processing of segmentation by the ATLSWE model is to strip the skull region by using the mathematical morphology operators [22]. The selection of threshold parameters must be performed for segmentation of the WM and GM tissues in a brain and the flowchart is shown in figure (fig1). Because the ATLSWE model has different meaning from the methodology of Chan and Vese model [19], the Chan and Vese model is described in the next section to compare with the ATLSWE model.

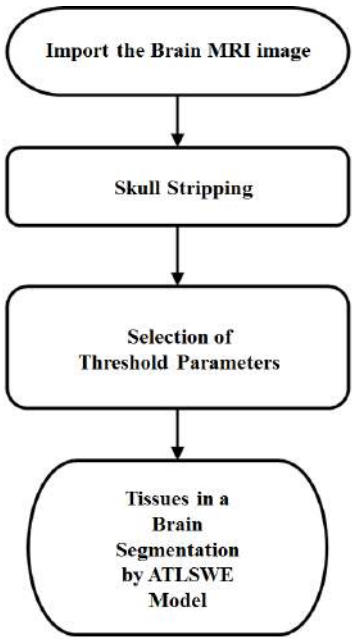


**Fig. 1:** Flow chart image segmentation of the tissues in brain.

## 3 Chan and Vese Model

Chan and Vese model is an active contour model for segmentation of objects without explicit edges in images. The red active contour $\Gamma$ evolves to separate an image into two regions as shown in figure (2a). One region is inside $\Gamma$ and the other region is outside $\Gamma$. The curve $\Gamma_{OPT}$ is located at the boundary between objects and background and finally the red active contour meets the curve $\Gamma_{OPT}$ as shown in figure (2b).

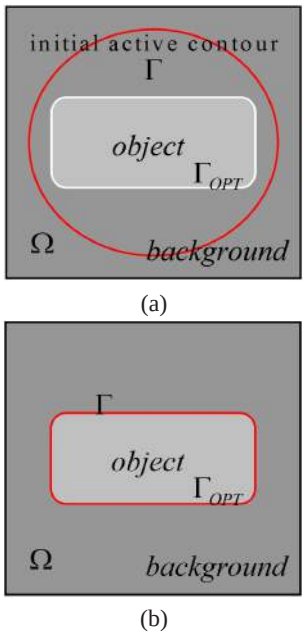


**Fig. 2:** (a) Initial active contour $\Gamma$ and (b) boundary $\Gamma_{OPT}$ of the object.

The optimal location of active contour $\Gamma$ is minimization of energy that is defined by the sum of the

intensity variance of inner and outer regions. The active contour $\Gamma$ separates an image into two regions and its best location is at force equilibrium state in an image force filed.

Intensity $\mu_0$ of an image is a function jointed by two intensity functions $u_0^i$ and $u_0^o$ that are inside and outside regions of the contour $\Gamma$. Functional $E(\overrightarrow{C})$ is defined by equation (1).

$$E(\overrightarrow{C}) = \int_{inside(\Gamma)} (u_0 - c_1)^2 + \int_{outside(\Gamma)} (u_0 - c_2)^2 + \mu |\Gamma|, \quad (1)$$

where $c_1$ and $c_2$ are the averages of $u_0^i$ and $u_0^o$, $\mu$ is a positive parameter and $|\Gamma|$ is the length of the evolving curves. The active contour $\Gamma$ captures the boundaries of objects $\Gamma_{OPT}$ when the functional $E(\Gamma)$ is minimized.

The evolution curves can be represented by the zero-level lines of a surface function $\phi$ in $R^3$ and the approach $\overrightarrow{C} = \{(x,y)|\phi(x,y) = 0\}$ is called level set formulation. Chan and Vese substitute the level set function $\phi$ into the functional $E(\overrightarrow{C})$.

$$\begin{aligned} E(c_1,c_2,\phi) &= E_1(c_1,c_2,\phi) + E_2(c_1,c_2,\phi) + \mu l(\phi) \\ &= \int_\Omega (u_0 - c_1)^2 H(\phi) dxdy \\ &+ \int_\Omega (u_0 - c_2)^2 (1 - H(\phi)) dxdy \\ &+ \mu \int_\Omega |\nabla H(\phi)| dxdy, \end{aligned} \quad (2)$$

where $\Omega$ is the total region in the image, $\phi$ is a level set function and $H$ is a Heaviside function and $c_1$ and $c_2$ are average values of intensity $u_0$ inside and outside regions of $\Gamma$ . By variation calculus, Chan and Vese model uses the following conditions

$$\frac{\partial E_1}{\partial c_1} = \frac{\partial E_2}{\partial c_2} = 0$$

to obtain the Euler-Lagrange equation (3.a) and the evolution equation (3.b) ,

$$\delta_\varepsilon(\phi)\left(\mu \frac{\nabla\phi}{|\nabla\phi|} - (u_0 - c_1)^2 + (u_0 - c_2)^2\right) = 0, \quad (3.a)$$

$$\frac{\partial \phi}{\partial t} = \delta_\varepsilon(\phi)\left(\mu \frac{\nabla\phi}{|\nabla\phi|} - (u_0 - c_1)^2 + (u_0 - c_2)^2\right), \quad (3.b)$$

where $\mu$ is a parameter and $\delta_\varepsilon = H'_\varepsilon$ is a delta function of the derivative of an approximate Heaviside function $H_\varepsilon$ . The symbols $c_1$ and $c_1$ can be formulated as following:

$$c_1 = \frac{\int_\Omega u_0 H(\phi) dxdy}{\int_\Omega H(\phi) dxdy}, \; c_2 = \frac{\int_\Omega u_0 (1 - H(\phi)) dxdy}{\int_\Omega (1 - H(\phi)) dxdy}. \quad (4)$$

Figure (3a) is a synthetic image to show the drawbacks of the Chan-Vese model. The synthetic image has multiple regions with different grey level and our desired ROI (blue area) as is shown in figure (3b). The region inside the red curve in figure (3c) is the segmentation result and it does not match our desired blue area.

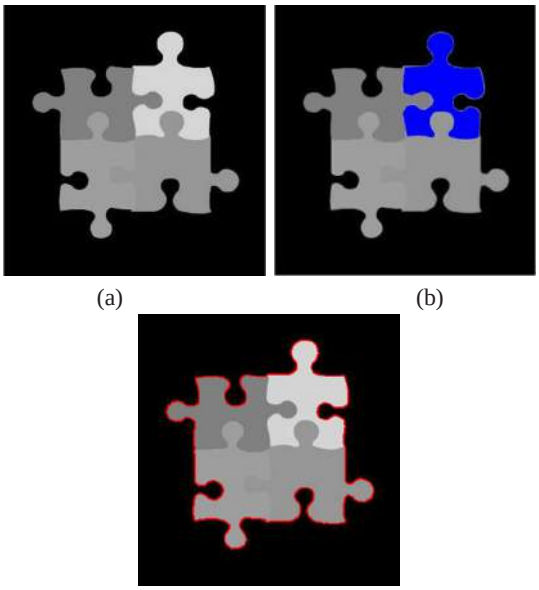

(a) (b)

(c)

**Fig. 3:** (a) The synthetic image (b) ROI (blue) and (c) segmentation result (inside red curve).

The location of the red active contour is decided by $c_1$ and $c_2$ and they are automatically computed by the equation (4). The results of $c_1$ and $c_2$ are not satisfied to locate the red active contour to the desire position around the blue area. The parameters $c_1$ and $c_2$ should be adjusted to locate the active contour at the desired position.

## 4 Mathematical Proof and Parameters of ATLSWE Model

Mathematical Proof of ATLSWE Model is given to show the difference between the ATLSWE Model and Chan-Vese model.

### *4.1 Proof of The ATLSWE Model*

These two models have the same Euler-Lagrange equation (3), but their conditions and derivation process of the equations are different. The mathematical proof of the ATLSWE model can show that $c_1$ and $c_2$ are parameters to be selected for achieving the segmentation results.

The Euler-Lagrange equation of the ATLSWE model can be derived by calculus of variations and the functional $E(c_1,c_2,\phi)$ in the equation (2). Consider a function $\phi=\phi^*+t\psi$ and it equals to $\phi^*$ plus a variation $t\psi$. The function $\psi$ is an arbitrary function with a boundary condition $\psi|_{\partial\Omega}=0$ and the function $\phi^*$ is a function when the independent variable $t$ is zero. The necessary condition $\delta E|_{\phi=\phi^*}=0$ is used to find the function $\phi^*$. The necessary condition $\delta E|_{\phi=\phi^*}=0$ is equivalent to the following condition that functional $E$ is differentiated with respect to independent variable $t$.

$$\left.\frac{dE}{dt}\right|_{t=0}=0. \tag{5}$$

In equation (2), $E_1$ , $E_2$ and $l(\phi)$ are summarised as follows.

$$E_1(c_1,c_2,\phi)=\int_\Omega (u_0-c_1)^2H(\phi)dxdy, \tag{6.a}$$

$$E_2(c_1,c_2,\phi)=\int_\Omega (u_0-c_2)^2\left(1-H(\phi)\right)dxdy. \tag{6.b}$$

$$\begin{aligned} l(\phi)&=\int_\Omega |\nabla H(\phi)|\,dxdy\\ &=\int_\Omega \delta_\varepsilon|\nabla\phi|\,dxdy. \end{aligned} \tag{7}$$

The left side of equation (5) can be formulated as follow.

$$\left.\frac{dE}{dt}\right|_{t=0}=\frac{dE_1}{dt}+\frac{dE_2}{dt}+\mu\frac{dl(\phi^*)}{dt}. \tag{8}$$

The first and second terms in the equation (8) can be derived to obtain the equations (9.a) and (9.b).

$$\left.\frac{dE_1}{dt}\right|_{t=0}=\frac{\partial E_1}{\partial c_1}\frac{\partial c_1}{\partial\phi}\frac{\partial\phi}{\partial t}+\frac{\partial E_1}{\partial\phi}\frac{\partial\phi}{\partial t}, \tag{9.a}$$

$$\left.\frac{dE_2}{dt}\right|_{t=0}=\frac{\partial E_2}{\partial c_2}\frac{\partial c_2}{\partial\phi}\frac{\partial\phi}{\partial t}+\frac{\partial E_2}{\partial\phi}\frac{\partial\phi}{\partial t}. \tag{9.b}$$

Substituting equation (7) into the third term in equation (8), the equation (10) is obtained.

$$\mu\frac{dl(\phi^*)}{dt}=-\iint_\Omega \mu\delta E(\phi^*)\nabla\cdot\frac{\nabla\phi}{|\nabla\phi|}\psi dxdy. \tag{10}$$

The conditions of the ATLSWE Model are

$$\frac{\partial c_1}{\partial\phi}=0 \text{ and } \frac{\partial c_2}{\partial\phi}=0, \tag{11}$$

and they are different from the condition of the Chan and Vese model.

$$\frac{\partial E_1}{\partial c_1}=0 \text{ and } \frac{\partial E_2}{\partial c_2}=0.$$

Substitute conditions in equation (11) into equations (9.b) and (9.b), the following equations are obtained by using equations (6.a) and (6.b).

$$\left.\frac{dE_1}{dt}\right|_{t=0}=\frac{\partial E_1}{\partial\phi}\frac{\partial\phi}{\partial t}=\int_\Omega (u_0-c_1)^2\delta(\phi^*)\psi dxdy, \tag{12.a}$$

$$\left.\frac{dE_2}{dt}\right|_{t=0}=\frac{\partial E_2}{\partial\phi}\frac{\partial\phi}{\partial t}=\int_\Omega (u_0-c_2)^2\delta(\phi^*)\psi dxdy. \tag{12.b}$$

Substituting equations (10), (12.a) and (12.b) into equation (5), the equation (12) is obtained.

$$\iint_\Omega \delta_\varepsilon(\phi^*)\left[\Phi+U\right]\psi dxdy=0, \tag{13}$$

where $\Phi=-\mu\nabla\cdot\frac{\nabla\phi^*}{|\nabla\phi^*|}$ and $U=(u_0-c_1)^2-(u_0-c_2)^2$. Because the function $\psi$is an arbitrary function, the part embraced by parentheses should be equal to zero.

$$\delta_\varepsilon(\phi^*)\left[-\mu\nabla\cdot\frac{\nabla\phi^*}{|\nabla\phi^*|}+(u_0-c_1)^2-(u_0-c_2)^2\right]=0, \tag{14.a}$$

The evolution equation of level set function is as follow.

$$\frac{\partial\phi}{\partial t}=\delta_\varepsilon(\phi^*)\left[\mu\nabla\cdot\frac{\nabla\phi^*}{|\nabla\phi^*|}-(u_0-c_1)^2+(u_0-c_2)^2\right]. \tag{14.b}$$

The equation (14.a) is the same as the equation (3.a) but they do not satisfy the same condition. According to the conditions in equation (11), the parameters $c_1$ and $c_2$ are constants. The same functional with different conditions obtain the same Euler-Lagrange equation.

## *4.2 Parameters of The ATLSWE Model*

Parameters of the ATLSWE are defined in this section. Ignoring the curvature effect and substituting $\mu=0$ into equation (14.b), equation (15) is obtained as follow.

$$\frac{\partial\phi}{\partial t}=\delta_\varepsilon(\phi)\left(-(u_0-c_1)^2+(u_0-c_2)^2\right). \tag{15}$$

The equation (15) is changed to equation (16).

$$\frac{\partial\phi}{\partial t}=-2\delta_\varepsilon(\phi)\left((c_2-c_1)\left[u_0-\frac{c_1+c_2}{2}\right]\right). \tag{16}$$

In the equation (16), the constant values of $c_1$ and $c_2$ decide the location of the active contour $\Gamma$. Since the value of $\frac{c_1+c_2}{2}$ can also decide the location of the active contour $\Gamma$, we choose $c_0=\frac{c_1+c_2}{2}$ as a parameter. An image segmentation example is to show different

segmentation capability of Chan-Vese model and the ATLSWE model. Figure (fig4a) is a synthetic image has sixteen squares with increasing gray levels from left to right and top to bottom. Segmentation result by Chan-Vese model is shown in figure (fig4b). There is no choice for ROI selection by Chan-Vese model. All sixteen squares are enclosed by the blue lines. The ATLSWE model can capture desired ROI as segmented areas when the value $c_0$ of evolution equation (16) is 155. The value $c_0$ can be chosen to select the desired square areas. Only six squares are enclosed by the blue lines are shown in figure (fig4c).

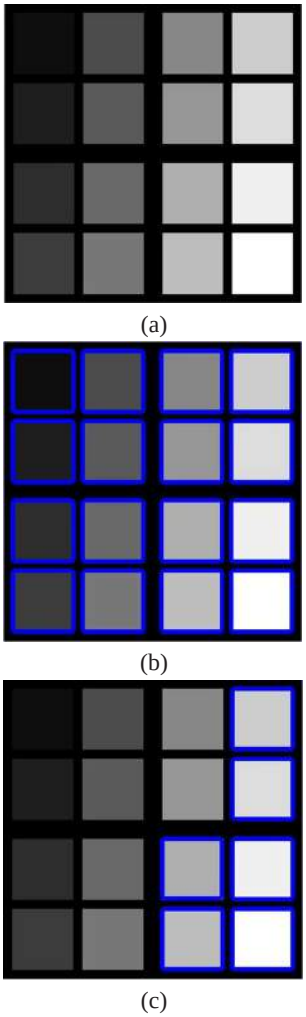

**Fig. 4:** (a) Synthetic image (b) segmentation result by Chan-Vese model, and (c) segmentation result by equation (16) with $c_0 = 155$.

## 5 Results and Discussions

Segmentation by ATLSWE model for the WM, and GM tissues needs parameters $LT$ and $UT$ that are boundaries of the intervals of intensities of the ROI. Automatic selection of lower and upper threshold parameters is important for the accuracy and efficiency segmentation of brain image.

### *5.1 Synthetic Brain image Segmentation*

GM tissue in a brain is a band region with both outer and inner contours and it needs two level set function $\phi_1$ and $\phi_2$ to find outer and inner contours. Substituting $\phi = \phi_1$ into the equation (16) and replacing $\frac{c_1+c_2}{2}$ with a symbol $c_3$, equation (17.a) is obtained.

$$\frac{\partial \phi_1}{\partial t} = -2\delta_\varepsilon(\phi_1)((c_2-c_1)(u_0-c_3)). \qquad (17.a)$$

Substituting $\phi = \phi_2$ into the equation (16) and replacing $c_1$, $c_2$ and $\frac{c_1+c_2}{2}$ with symbols $c_4$, $c_5$ and $c_6$, equation (17.b) is obtained.

$$\frac{\partial \phi_2}{\partial t} = -2\delta_\varepsilon(\phi_2)((c_5-c_4)(u_0-c_6)). \qquad (17.b)$$

Figure (fig5a) is a synthetic brain image with gray region as a desired ROI. The gray level of the gray region is in the interval between Lower Threshold $c_3$ and Upper Threshold $c_6$.

Using $\phi = \phi_1$ and $c_3$, the active contour captures the outer contour of ROI. Using $\phi = \phi_2$ and $c_6$, the active contour captures the inner contour of ROI. Figure (fig5b) shows the ROI region between the red inner contour and red outer contour.

### *5.2 Physical Brain image Segmentation*

The popular image segmentation method such as Fuzzy C-Means (FCM) algorithm [7,8] is not suitable for the segmentation of brain MR image. Fuzzy C-Means (FCM) algorithm is one kind of clustering method to solve unsupervised learning problems. The FCM algorithm used for image segmentation method is to group pixels in an MRI image according to their gray level without considering the location of pixels. That is why the boundaries of the segmentation results are not continuous. Figure (fig6a) is a brain MRI image. Figure (fig6b) and (fig6c) are clustering results by FCM with group numbers 3 and 4. Figure (fig6d) and (fig6e) are enlarged pictures of rectangle areas in figure (fig6b) and (fig6c). In figure (fig6b), there are pixels with red, green and blue colours to represent tissues of WM, CSF, GM and background. In figure (fig6c), there are pixels with red, green, blue and yellow colours.

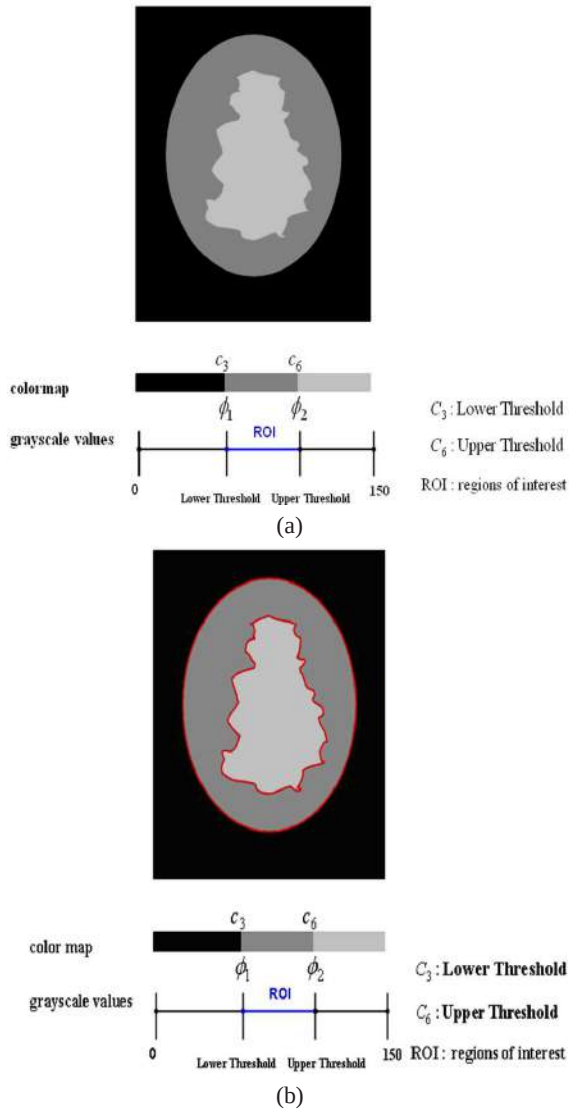


**Fig. 5:** Synthetic brain image with gray region as a desired ROI.

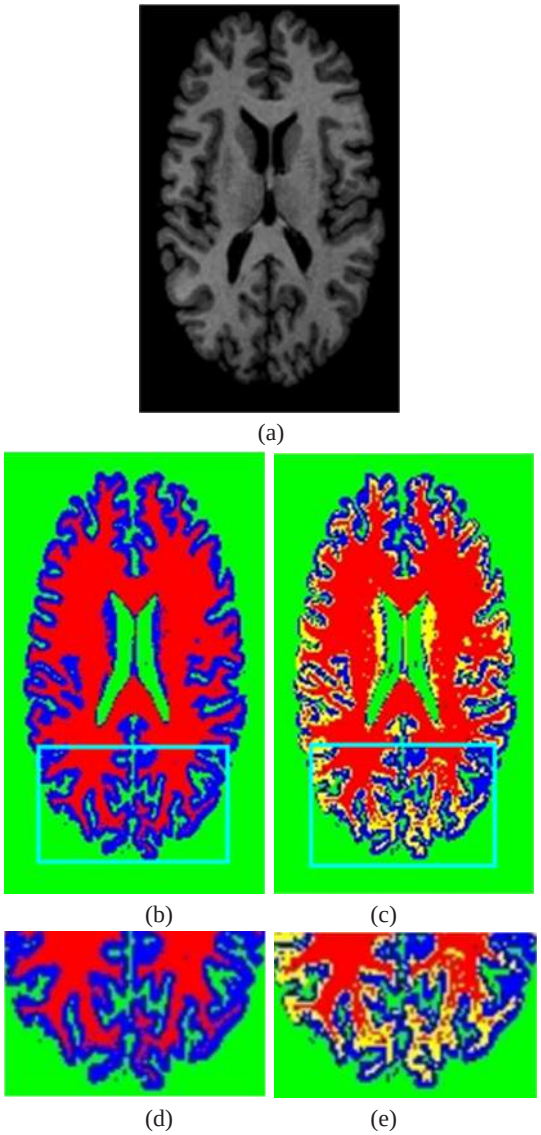


**Fig. 6:** Clustering results of brain image (a) by FCM with groups (b) 3 and (c) 4 with (d) and (e) are enlarged pictures of rectangle in (b) and (c).

In this paper, the FCM algorithm is not used as a segmentation method, but it is used to determine the Upper Threshold ($UT$) and Lower Threshold ($LT$). To locate smooth boundaries of WM and GM is the benefit of the ATLSWE model using the parameter selection algorithm by Fuzzy C-Means algorithm. In figure (fig6b), there are three regions marked by three colours and their intensity distributions of pixels are listed in Table (t1). The interval of the intensity for green, blue and red groups are $(0,29)$, $(29,83)$ and $(83,138)$. In Table (t1) the intervals of GM and WM are $(b,B)$ and $(r,R)$. The intensity distributions of pixels in the four regions marked by four colours as shown in figure (fig6c) are listed in Table 2. In Table 2, the intervals of GM and WM are $(b,B)$ and $(r,R)$. The yellow interval is $(y,Y)$ in Table 2.

As shown in table 2, the intervals belong to WM, GM, CSF and Background are changed comparing to the intervals in table 1. The intervals of the blue and red green groups in table 2 are smaller than in table 1 because some pixels in red and blue groups will be reassigned into the yellow group in table 2. We know the interval of GM is $(29,83)$ and the interval of WM is $(83,138)$ in table 1; on other hand, the interval of GM is $(24,63)$ and the interval of WM is $(94,138)$ in table 2. It is reasonable to guess the optimal lower limit of WM is between 63 and 94, but it may not be 83 and can not be obtained by FCM. As the reasons, FCM can not segment the MR brain image more accurately.

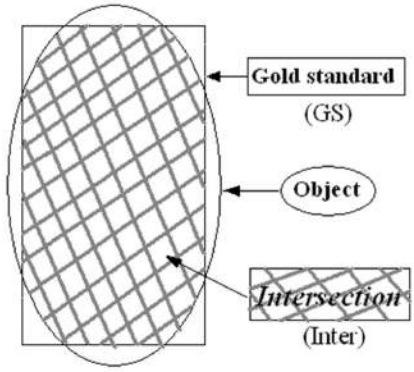


**Fig. 7:** Diagram of Gold standard, object and intersection parts.

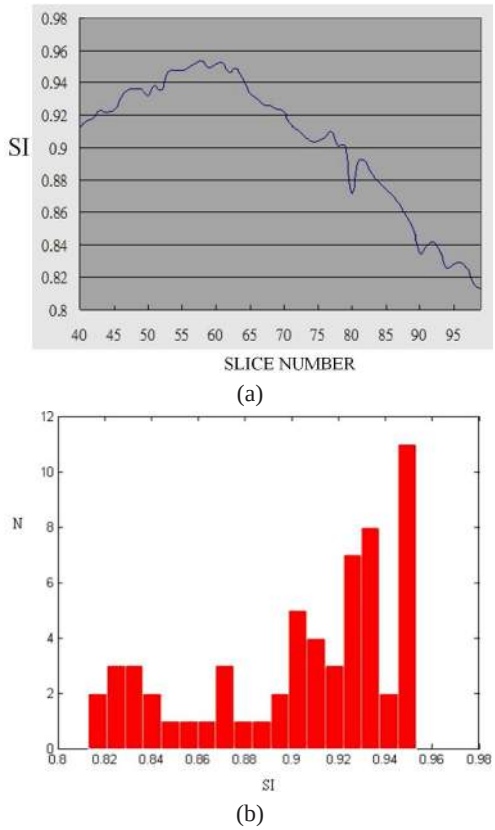


**Fig. 8:** (a) The similarity indices curve and (b) histogram obtained of the 40$^{th}$ to 99$^{th}$ MR image segmentations.

The selection of threshold parameters, $UT$ and $LT$, for WM, GM and CSF tissues is listed by steps as follows:

(1) Set $c = 3$, then obtain blue interval $[b,B]$ and red interval $[r,R]$.
(2) Set $c = 4$, then obtain yellow interval $[y,Y]$.
(3) Select Lower Threshold $LT$ and Upper Threshold $UT$ for WM and GM tissues.

(a) (b) (c)

**Fig. 9:** (a) The 60$^{th}$ slice MRI image (b) with the golden standard and (c) segmented object by ATLSWE.

**Table 1:** Three groups are classified by FCM as shown in figure **??**.

| Tissues | CSF & Background | GM | WM |
|---|---|---|---|
| Colours | Green | Blue | Red |
| Lower Threshold | $g = 0$ | $b$ | $r$ |
| Upper Threshold | $G = 29$ | $B$ | $R$ |
| Intervals | $(g,G) = (0,29)$ | (29,83) | (83,138) |

**Table 2:** Four groups are classified by FCM as shown in figure **??**.

| Tissues | CSF & Background | GM | GM/ WM | WM |
|---|---|---|---|---|
| Colours | Green | Blue | Yellow | Red |
| Lower Threshold | $g = 0$ | $b = 24$ | $y = 63$ | $R = 94$ |
| Upper Threshold | $G = 24$ | $B = 63$ | $Y = 94$ | $R = 138$ |
| Intervals | $(0,24)$ | (24,63) | (63,94) | (94,138) |

The selection of $UT$ and $LT$ is necessary to investigate Table 1 and 2. In Table 1, the intervals of CSF&Background, GM and WM tissues are $(g,G)$, $(b,B)$ and $(r,R)$ the interval of is. The yellow interval is $(y,Y)$ in table 2.

- Selection $UT$ and $LT$ for WM

Let $UT = R$ and $LT$ is selected by the following rule:

$$\text{IF } B > y \text{ THEN } LT = (B+y)/2 \text{ ELSE } LT = B$$

The rule can be transformed to a decision function by $LT$ in equation (18) where $H(x)$ is a Heaviside function or unit

step function defined as follow:

$$H(x) = \begin{cases} 1, x > 0, \\ 0, x \leq 0, \end{cases}$$

and

$$LT = \left[ \frac{(B+y) \times H(B-y) + 2B \times [1 - H(B-y)]}{2} \right]. \quad (18)$$

- Selection $UT$ and $LT$ for GM

Let $UT = B$ and $LT$ is selected by the following rule:

$$\text{IF } b < G \text{ THEN } LT = (G+b)/2 \text{ ELSE } LT = G$$

The rule can be transformed to a decision function $LT$ in equation (19) by Heaviside function .

$$LT = \left\{ \frac{2G \times H(b-G) + (b+G)\,[(1 - H(b-G)]}{2} \right\}. \quad (19)$$

(a) (b) (c)

**Fig. 10:** The 94th slice MRI image (b) with the golden standard and segmented object and (c) segmented object by ATLSWE.

## Accuracy Evaluation

The segmentation results of GM in the mrGray software are used as the ground truth to be segmentation standard for evaluating the accuracy of the segmentations of GM. Similarity index (SI) [23] is defined for evaluating accuracy of digital image[24,25] segmentation methods. Since SI is a measure of the correctly classified tissue area, then SI is defined as follow:

$$\text{SI} = \frac{2 \times Inter}{GS + Object}, \quad (20)$$

where GS denotes gold standard that is the ground truth of the WM segmentation and Object is the segmented result and Inter denotes the intersection of the ground truth and Object. The diagram of Gold standard, object and intersection parts is shown in figure (fig7).

The segmentation results of sixty images with slice numbers between the 40th and 99th by ATLSWE model are compared with the gold standard results to evaluate accuracy. The *SI* values defined in the equation (20) are calculated and shown in figure (fig8a) with the maximum 0.95307 and minimum 0.8131. A histogram of SI is shown in the figure (fig8b) with the mean value 0.90311 and the variance 0.042049. The parameter "N" in the figure (fig8b) is the times of SI values appeared.

The 60th and the 94th slice MRI images are shown in figure (fig9a) and (fig10a) and ground truth are in figure (fig9b) and (fig10b). The value of the similarity index SI

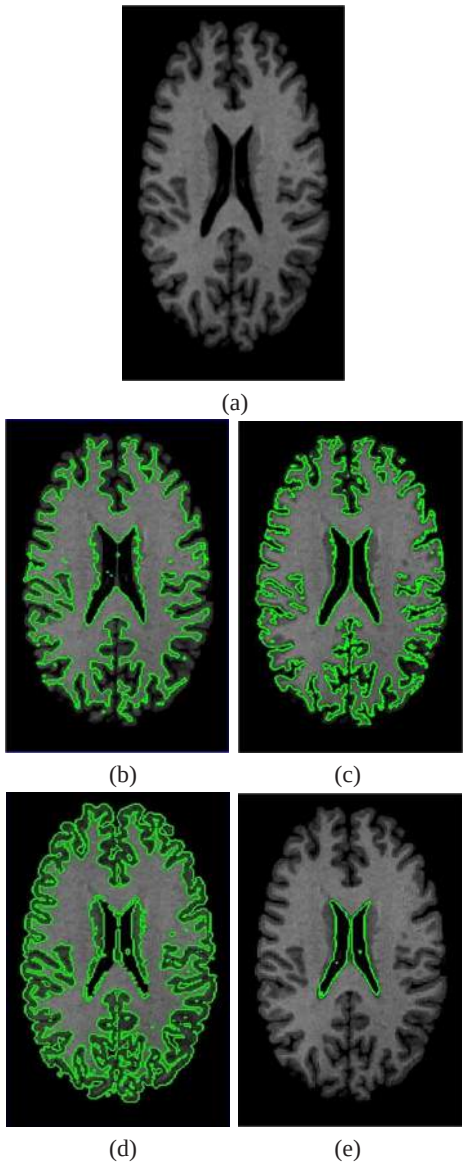

(a)

(b) (c)

(d) (e)

**Fig. 11:** (a)Original image, the result segmented (b) by Chan-Vese model and by ATLSWE Model with (c) $LT = 83$, $UT = 140$, (d) $LT = 27$, $UT = 83$ (e) $LT = 0$, $UT = 27$.

of the segmentation results in figure (fig9c) and figure (fig10c) are 0.9515 and 0.8252. The value 0.9515 is larger than mean value of SI (0.90311). The value 0.8252 is smaller than mean value of SI.

As shown in the center of figure (fig10b), the sup colliculus does not appear in the golden standard, but it appears in the segmented object as shown in the right of figure (fig10c). Although the SI value of $94^{th}$ image is smaller than the mean value of SI, but the outer contours of the white mater in figure (fig10b) and figure (fig10c) are almost the same. For the purpose of three dimensional surface reconstruction of WM, the segmentation result is also very useful.

Figure (fig11a) is the original brain MR image and figure (fig11b) is the segmented result of Chan-Vese model but it does not meet our desired result. Figure (fig11c), (fig11d) and (fig11e) show the WM, GM and CSF segmented results by ATLSWE Model with threshold parameters with (c) $LT = 83$, $UT = 140$, (d) $LT = 27, UT = 83$ (e) $LT = 0, UT = 27$.

## 6 Conclusions and future work

This paper proposed an ATLSWE model for automatic brain image segmentations. The segmented images of GM and WM tissues obtained from $40^{th}$ to $99^{th}$ MR slice of images in the mrGray software are used to test the performance of the ATLSWE model. The similar index is used for the accuracy evaluation of the image segmentation results. The statistic accuracy of the ATLSWE model by evaluation with the similar index has mean 0.90311 and the variance 0.042049. The proposed ATLSWE model can automatically and accurately segment the tissues of the brain MRI images. The ATLSWE model can be also used for PET or CT brain image segmentations.

## Acknowledgement

The authors would like to thank the National Science Council, R.O.C., for partially supporting this work under grant numbers (NSC 99-2115-M-324 - 001) and (NSC 100-2115-M-324 - 001).

## References

[1] Dhawan, A.P., Medical Image Analysis, John Wiley Publications and IEEE Press. (2003), 175-176.

[2] Morrison, M., Attikiouzel, Y., A probabilistic neural network based image segmentation network for magnetic resonance images. In Proc. Conf. Neural Networks. Vol. 3. (1992), 60-65.

[3] Ozkan, M., Dawant, B., Maciunas, R., Neural-network-based segmentation of multimodal medical images: a comparative and prospective study. IEEE Trans. Med. Imaging. Vol. 12. (1993), 534-544.

[4] Kollokian, V., Performance analysis of automatic techniques for tissue classification in MRI of the human brain. Master's thesis, Concordia University, Montreal, Canada. (1996).

[5] Wang, Y., Adah, T., Kung, S.-Y., Quantification and segmentation of brain tissues from MR images: A probabilistic neural network approach. IEEE Transactions on Image Processing. (1998), 7 (8), 1165-1181.

[6] Bezdek, J.C., Hall, L.O. and Clarke, L.P., Review of MR Image Segmentation Techniques Using Pattern Recognition. Medical Physics. 20(4), (1993), 1033-1048.

[7] Bezdek, J.C., Pattern Recognition with Fuzzy Objective Function Algorithms. Plenum Press, New York. (1981).

[8] Dunn, J.C., " A Fuzzy Relative of the ISODATA Process and Its Use in Detecting Compact Well-Separated Clusters". Journal of Cybernetics. Vol.3. (1974), 32-57.

[9] Kass, M., Witkin, A., and Terzopoulos, D. , "Snakes - Active Contour Models". International Journal of Computer Vision. (1987), 1(4):321-331.

[10] Osher S. and Sethian J.A., Fronts propagating with curvature dependent speed: Algorithms based on Hamilton-Jacobi formulations. Journal of Computational Physics. (1988), 79(1), 12-49.

[11] Sethian, J. A., Level set methods and fast marching methods: evolving interfaces in computational geometry, fluid mechanics, computer vision and materials science. Cambridge University Press, Cambridge, UK. (1999).

[12] Hoffmann, T. J., Chung, M. K., Dalton, K. M., Alexander, A. L.,Wahba, G., Davidson, R. J.,. Subpixel curvature estimation of the corpus callosum via splines and its application to autism. 10th Annual Meeting of the Organization for Human Brain Mapping. (2004). http://www.stat.wisc.edu/ mchung/papers/HBM2004/HBM2004thomas.html

[13] Tohka, J., Zijdenbos, A., Evans, A. C., Fast and robust parameter estimation for statistical partial volume models in brain MRI. NeuroImage. (2004), 23 (1), 84-97.

[14] Mumford, D., Shah, J., Boundary detection by minimizing functionals. In IEEE Computer Society Conference on Computer Vision and Pattern Recognition (CVPR). (1985), 22-26.

[15] Malladi, R., Sethian, J.A., Vemuri, B.C., Shape modeling with front propagation: A level set approach. IEEE Trans. on Pattern Analysis and Machine Intelligence. Vol. 17. (1995), 158-175.

[16] Lefohn, A., Kniss, E., Hansen, J., C., and Whitaker, R., "Interactive deformation and visualization of level set surfaces using graphics hardware". In IEEE Visualization. (2003), 497-504.

[17] Zchang, Z.U., and Hsu, C.Y., Automatic Segmentation by Threshold Level Set Method with Adaptive Parameters. CVGIP 2005 conference in Taiwan. (2005).

[18] N. Otsu, A threshold selection method from gray-level histograms. IEEE Transactions on Systems, Man, and Cybernetics. Vol. 9, No. 1. (1979), pp. 62-66.

[19] Chan, T.F., Vese, L.A., Active Contours Without Edges. IEEE Trans. on Image Processing. (2001), 10(2), 266-277.

[20] Teo, P.C., Sapiro, G. and Wandell, B.A., Creating connected representations of cortical grey matter for functional MRI visualization. IEEE Transactions on Medical Imaging, Vol. 16. (1997), 852-863.

[21] Wandell, B., Chial S., and Backus, B., Visualization and Measurement of the Cortical Surface. Journal of Cognitive Neuroscience, Vol. 12, No. 5. (2000), 739-52.
[22] Kapur, T., W. Eric L. Grimson, William M. Wells III, Kikinis. R., Segmentation of brain tissue from magnetic resonance image. Medical Image Analysis, Vol. 1, No. 2. (1996), pp 109-127.
[23] Zijdenbos, A.P., Dawant, B.M., Margolin, R.A., and Palmer, A.C. , Morphometric analysis of white matter lesions in MR images: method an validation. IEEE Trans. Med. Imaging, Vol. 13. (1994), 716-724.
[24] Latif, A., An Adaptive Digital Image Watermarking Scheme using Fuzzy Logic and Tabu Search , Journal of Information Hiding and Multimedia Signal Processing, Vol. 4, No. 4, (2013),250-271.
[25] Feng,H.M., Horng, J.H., and Jou, S.M., Bacterial Foraging Particle Swarm Optimization Algorithm Based Fuzzy-VQ Compression Systems, Journal of Information Hiding and Multimedia Signal Processing, Vol. 3, No. 3,(2012),227-239.

**Ming Zhao** received the Master degrees in computer aided Instruction from Huazhong Normal University, China in 2006, Now he is Ph.D candidate in Harbin Institute of Technology Shenzhen Graduate School, he is currently an associate professor in Yangtze University, China. His research interests include computational intelligence, image and signal processing, pattern recognition etc. He is an IEEE Senior Member.

**Hsiao-Yu Lin** received the Master degrees in Applied Mathematics from Chung-Hsing University, Republic of China in 2008. Now she works in Winbond Electronics Corporation and her research interests are image processing.

**Chih-Hung Yang** received a Master degree in 2004, and Ph.D. degree in 2009 both in the Department of applied mathematics from National Chung-Hsing University at Taichung, Taiwan. His research interests are Partial Differential Equation and Numerical Analysis for medical image processing. Now, he works at Automotive Research & Testing Center, Changhwa, Taiwan, R.O.C.

**Chih-Yu Hsu** received the M.S. degree in 1993, and Ph.D. degree in 1997, both in the Department of applied Mathematics from National Chung-Hsing University at Taichung, Taiwan. At present, he is on the faculty of the department of information & communication Engineering, ChaoYang University of Technology, Taichung Taiwan, R.O.C, where he is currently an associate professor. His research interests include image and signal processing.

**Jeng-Shyang Pan** received the B.S. degree in electronic engineering from the National Taiwan University of Science and Technology, Taipei, Taiwan, in 1986, the M.S. degree in communication engineering from the National Chiao Tung University, Hsinchu, Taiwan, in 1988, and the Ph.D. degree in electrical engineering from the University of Edinburgh,Edinburgh, U.K., in 1996. He is currently a Professor in the Department of Electronic Engineering, National Kaohsiung University of Applied Sciences, Kaohsiung, Taiwan. He is also the Doctoral Advisor with the University of South Australia and Harbin Institute of Technology, Harbin, China. He has authored or coauthored more than 270 papers, 92 of which are indexed by the Science Citation Index. He is a member of the editorial board of the International Journal of Innovative Computing, Information and Control, the Lecture Notes in Computer Science Transactions on Data Hiding and Multimedia Security, the International Journal of Hybrid Intelligent System, the Innovative Computing, Information and Control Express Letters, the International Journal of Computer Sciences and Engineering Systems, and the Journal of Information Hiding and Multimedia Signal Processing. He is the Founder of the International Conference on Intelligent Information Hiding and Multimedia Signal Processing and the International Conference on Innovative Computing, Information, and Control. His current research interests include soft computing, information security, and signal processing.

**Meng-Ju Lin** received a Master degree in 2004, and Ph.D. degree in 2011 both in the Department of applied mathematics from National Chung-Hsing University at Taichung, Taiwan. His research interests are Statistics and Financial Analysis.